Imaging Topography and Viscoelastic Properties by Constant Depth Atomic Force Microscopy

Michael R. P. Ragazzon[1], J. Tommy Gravdahl[1]

Abstract— **Identification of mechanical properties of cells is known to be an effective tool for medical diagnosis, and holds potential for future developments in treatment of various diseases. In this paper a novel method for identification of viscoelastic properties of a soft sample using atomic force microscopy in dynamic mode is presented. The estimation scheme is based on parameter identification of a lumped spring-damper system model. The estimator guarantees exponentially fast parameter convergence. The indentation depth of the tip into the sample must be constant for viscoelastic properties to be consistent during a scan. A depth controller is designed to keep the indentation constant by utilizing the online estimates of the sample spring constant and topography. Simulations show the effectiveness of the presented method.**

I. INTRODUCTION

Greater understanding of cell mechanics of cancerous cells hold significant potential for developments in disease diagnostics and treatments [1], and it has been shown that cancer drugs and chemotherapy significantly influence mechanics of cells. Various tools have been used to identify mechanical properties of cells including micropipette aspiration, optical tweezers, and magnetic twisting cytometry [2], [3]. More recently, atomic force microscopy (AFM) has become an increasingly important tool for identifying cell mechanics [4], [5], [6], [7]. AFM allows for high-resolution imaging of soft biological material in natural conditions and makes it possible to simultaneously perform topography and elasticity measurements.

AFM works by having a cantilever with a sharp tip attached suspended over the sample surface. As the tip touches the sample, the cantilever will be deflected. This deflection can be measured with resolutions of sub-nanometer levels. By moving the cantilever in the vertical direction keeping the deflection constant, while moving the sample in the lateral directions, the topography of the sample can be identified. In dynamic mode AFM the cantilever is forced to oscillate, then as the cantilever is brought closer to the sample the amplitude, phase, and frequency of the oscillations will change [8]. By demodulating these signals, such as the amplitude, this can then be used as the feedback signal [9], [10].

A considerable amount research with AFM has been performed on identifying elasticity modulus of cells and other biological materials [11], [12], which are typically performed statically. That is, by indenting the sample at one or multiple number of points and measuring the deflection against the commanded cantilever position. Other approaches employ dynamic modes of AFM for identifying viscoelastic properties of the sample [13], [14], [15]. Such approaches require that the tip is in contact with the sample during the entire oscillation cycle. This is only possible for soft materials. With very stiff materials the tip would only intermittently be in contact with the sample. Although viscoelastic models are considerably simplified models of soft samples such as cells, these properties have been widely studied and clearly demonstrate correlations to diseases such as cancer [16].

In [17] a different technique was developed to identify viscoelastic properties. By employing a modeling- and identification scheme of the sample, the viscoelastic properties is found using control engineering tools. However, the mechanical properties are only identified at a discrete number of points by tapping in and out of the sample.

In this work we expand on the methodology in [17] and show how the viscoelastic properties can be gathered in a continuous fashion as the sample is scanned along the lateral axes. A key issue is how to identify and maintain a constant indentation depth into the sample which is critical for consistent measurements of the viscoelastic properties. The solution proposed here employs the online estimation of the spring constant and topography in a feedback loop to maintain constant depth. The cantilever is oscillated in dynamic mode to ensure persistency of excitation properties and thus convergence of the estimates.

The depth controller presented here has potential for replacing the traditional amplitude estimation feedback such as employed in [13], when scanning soft materials. The viscoelastic measurements are known to change with depth, and by scanning at constant depth consistency of the results is maintained.

In the next section a system model description of the viscoelastic sample is designed suitable for parameter identification. An estimator for the elastic (spring constant) and viscous (damping constant) properties, as well as the topography is devised in Section III. The estimates are then used in the constant depth controller essential for consistent results in Section IV. Simulations results are presented in Section V. Discussion and conclusions follow in Section VI–VII.

II. SYSTEM MODELING

In this section the sample dynamics, tip geometry, and cantilever dynamics are described and combined for a full

[1] M. R. P. Ragazzon and J. T. Gravdahl are with the Department of Engineering Cybernetics, Norwegian University of Science and Technology, Trondheim, Norway. E-mail: ragazzon@itk.ntnu.no, Tommy.Gravdahl@itk.ntnu.no

description of the system dynamics. This section largely follows the approach of [17].

The sample to be measured is modeled as a system of discrete spring-damper elements as illustrated in Figure 1. The elements are evenly distributed in the lateral xy-axes, and can be compressed in the vertical z-direction.

The interaction between the AFM cantilever and the sample is illustrated in Figure 2. The tip position along the xyz-axes is denoted by (X,Y,Z). The vertical tip position Z, the cantilever deflection D, and the controllable cantilever base position U are related by

$$Z = U - D. \tag{1}$$

Since the deflection D is measurable and U is controllable, all three signals are assumed to be available.

A. Tip Geometry

The cantilever tip is modeled as a sphere with tip radius R. The vertical position z_i of the spring-damper element i in contact with the tip is then given by

$$z_i = Z - \sqrt{R^2 - (X - x_i)^2 - (Y - y_i)^2} \tag{2}$$

$$\dot{z}_i = \dot{Z} \tag{3}$$

where x_i, y_i are the position of the element along the lateral axes, and $\dot{z}_i$ is the element velocity. It has been assumed that $\dot{X}$ and $\dot{Y}$ are much smaller than $\dot{Z}$. This is justified by the fact that the cantilever is oscillated at a high frequency near resonance resulting in a significant rate of change in Z, while the sample is scanned relatively slow in the lateral directions.

A spherical tip can be advantageous in use with soft, fragile samples [5], although if desired the equations (2)-(3) can easily be modified to handle different tip geometries. The tip geometry is only necessary for simulation purposes, as the parameter identification scheme does not require a tip model. However, the scaling of the identified parameters are dependent on the tip. Thus, if the radius is not known the values on the axis may be inaccurate, but the plots will appear equivalent.

B. Sample Force

The sample is modeled by viscoelastic elements. Thus, each element in contact with the tip provides a spring and a damping force. The force from element i can be described by

$$F_i = -k_i \bar{z}_i - c_i \dot{\bar{z}}_i \tag{4}$$

where k_i is the spring constant of element i, c_i is the damping constant, and $\bar{z}_i$ is the indentation of the tip into the element,

$$\bar{z}_i = z_i - z_i^0 \tag{5}$$

where z_i^0 is the rest-position of the element, or equivalently the sample topography at the position of the element.

The sample elements in contact with the tip is denoted by the active set $\mathbf{W}(X,Y,Z)$ which changes as the tip scans over the sample,

$$\mathbf{W} = \left\{ i : \bar{z}_i < 0 \wedge (X - x_i)^2 + (Y - y_i)^2 < R^2 \right\}. \tag{6}$$

The element i is thus only added to the active set if the tip is indenting it. This method could be extended to model the attractive forces near the surface by including elements with a small positive value of $\bar{z}_i$.

The sum of the forces acting on the cantilever tip from the sample is then given by

$$F_{\text{ts}} = \sum_{i \in \mathbf{W}} F_i. \tag{7}$$

C. Cantilever Dynamics

The cantilever dynamics can be described by a second-order harmonic oscillator [18]

$$M\ddot{Z} = KD + C\dot{D} + F_{\text{ts}} \tag{8}$$

$$= K(U - Z) + C(\dot{U} - \dot{Z}) + F_{\text{ts}} \tag{9}$$

where M is the effective mass of the cantilever, K is the cantilever spring constant, C is the cantilever damping constant, and F_{ts} is the sample force acting on the tip.

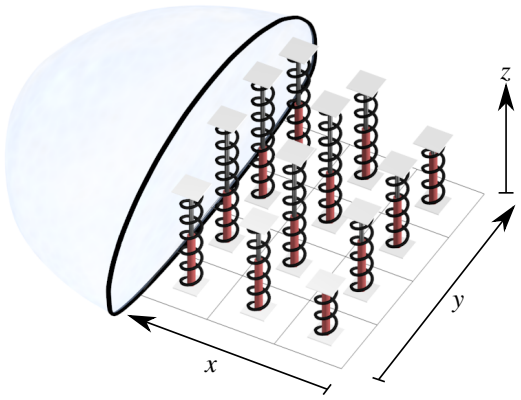

Fig. 1: The sample is modeled as spring-damper elements evenly spaced along the lateral axes.

III. Parameter Identification

The objective of the parameter identification scheme is to identify the sample properties given in the previous section. In this model the sample is fully described by the topography z^0, spring constant k, and damping constant c at every point in the lateral xy-axes. The relationship between the system dynamics and parameter estimator can be seen in the block diagram of Figure 3.

A. Parametric System Equations

The system equations need to be on a form suitable for parameter identification. Rewriting (9) and inserting for (4),(7) gives

$$M\ddot{Z} + K(Z - U) + C(\dot{Z} - \dot{U}) = \sum_{i \in \mathbf{W}} -k_i \bar{z}_i - c_i \dot{\bar{z}}_i \tag{10}$$

where the signals on the left hand side are known, and the right hand side contains the parameters to be estimated. It would be very challenging to determine all the sample parameters of each element individually. The problem is therefore simplified by rather trying to estimate the aggregate

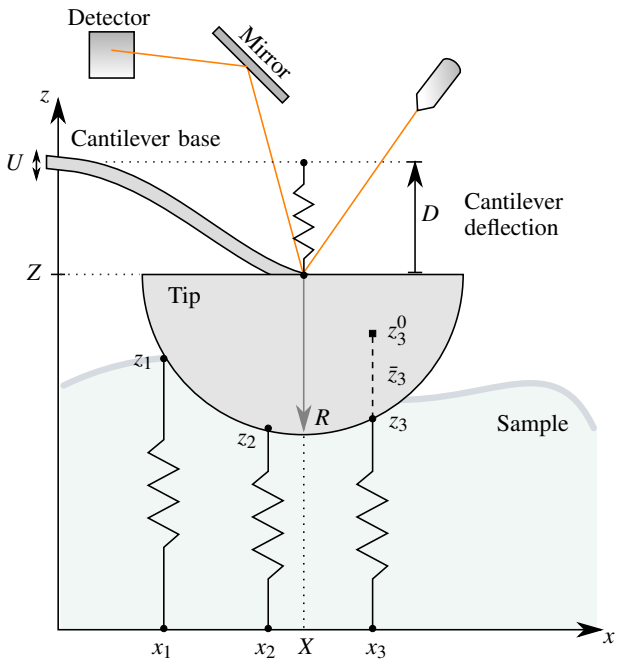

Fig. 2: Indentation of the tip into the sample.

spring constant k and damping constant c at the current tip position. The equation can thus be approximated by

$$M\ddot{Z}+K(Z-U)+C(\dot{Z}-\dot{U})=-k\bar{z}-c\dot{\bar{z}} \tag{11}$$

where c,k are now slowly-varying parameters as a function of the current lateral tip position (X,Y). By continuously estimating and logging c,k as the tip is scanned over the sample, the local viscoelastic properties of the sample are determined.

The indentation depth into the sample is given by

$$\bar{z}=Z-z^0 \tag{12}$$

where z^0 is the unknown sample topography at the current tip position. The topography needs to be determined in order to use $\bar{z}$ in (11), and we will include this as a parameter to be estimated. Rewriting (11) in the complex s-domain gives

$$Z(Ms^2+Cs+K)-U(Cs+K)=-k(Z-z^0)-csZ \tag{13}$$

which can be formulated as

$$w'=\begin{bmatrix} c \\ k \\ kz^0 \end{bmatrix}^T \begin{bmatrix} -sZ \\ -Z \\ 1 \end{bmatrix} \tag{14}$$

$$=\boldsymbol{\theta}^T\boldsymbol{\phi}' \tag{15}$$

where $\boldsymbol{\theta}$ is the unknown parameter vector to be estimated, $\boldsymbol{\phi}$ is the signal vector, and w is the measurable left hand side of (13). To avoid pure differentiation, both sides of (14) are filtered by a second order low-pass filter such as $1/\Lambda(s)=1/(\lambda s+1)^2$,

$$\frac{w'}{\Lambda}=\boldsymbol{\theta}^T\frac{\boldsymbol{\phi}'}{\Lambda} \tag{16}$$

$$w=\boldsymbol{\theta}^T\boldsymbol{\phi}. \tag{17}$$

This linear-in-the-parameters form is suitable for implementation of various parameter estimation methods such as given in [19]. The objective of the estimator is thus to find the unknown $\boldsymbol{\theta}$ given the signals w and $\boldsymbol{\phi}$.

B. Parameter Estimator

Many different estimation methods for the system (17) can be employed with similar stability and convergence properties. We have chosen the least squares method with forgetting factor from [19]. Due to the slowly varying nature of the parameters a forgetting factor is useful. The method is restated here for convenience,

$$\widehat{w}=\widehat{\boldsymbol{\theta}}^T\boldsymbol{\phi} \tag{18}$$

$$\varepsilon=(w-\widehat{w})/m^2 \tag{19}$$

$$m^2=1+\alpha\boldsymbol{\phi}^T\boldsymbol{\phi} \tag{20}$$

$$\dot{\widehat{\boldsymbol{\theta}}}=\mathbf{P}\varepsilon\boldsymbol{\phi} \tag{21}$$

$$\dot{\mathbf{P}}=\begin{cases}\beta\mathbf{P}-\mathbf{P}\frac{\boldsymbol{\phi}\boldsymbol{\phi}^T}{m^2}\mathbf{P}, & \text{if } \|\mathbf{P}\|\le R_0 \\ 0, & \text{otherwise}\end{cases} \tag{22}$$

$$\mathbf{P}(0)=\mathbf{P}_0 \tag{23}$$

where $\widehat{\boldsymbol{\theta}}=[\hat{c},\hat{k},\hat{k}\hat{z}_0]^T$ is the parameter estimate vector, α,β,R_0 are positive constants, and $\mathbf{P}\in\mathbb{R}^{3\times3}$ is the covariance matrix.

This method guarantees convergence of the error ε to zero given constant parameters $\boldsymbol{\theta}$. The parameters in our case are slowly-varying, but the error can be made arbitrarily small by reducing the scanning speed.

For the parameter vector $\widehat{\boldsymbol{\theta}}$ to converge to $\boldsymbol{\theta}$, the signal vector $\boldsymbol{\phi}$ needs to be persistently exciting (PE). Indeed, this is sufficient condition for exponential convergence of $\widehat{\boldsymbol{\theta}}\to\boldsymbol{\theta}$ [19]. For constant Z the signal is not PE, but it can be shown that for a single sinusoidal excitation of Z, the signal is PE. Since the system is linear, a sinusoidal excitation in U will result in a sinusoidal term in Z. Thus, the parameters will converge as long as the AFM is run in dynamic mode operation and scanning is performed sufficiently slow.

The following signal is suggested added to the commanded vertical position U while scanning to ensure PE conditions,

$$U_{exc}=a_1\sin(f_1 2\pi t)+a_2\sin(f_2 2\pi t) \tag{24}$$

where a_1,a_2 are suitably chosen constants, f_1 is near resonance frequency of the cantilever, and f_2 is lower frequency and used to provide additional excitation of the signal vector.

Since the topography estimate $\hat{z}_0$ is found after division by $\hat{k}$, the estimator should make sure $\hat{k}$ does not become zero. Since k is known to be strictly positive, a projection function such as from [20] can be used in the update law (21) to ensure $\hat{k}$ stays within provided limits.

IV. DEPTH CONTROLLER

Due to the spherical tip geometry the spring and damping forces acting on the tip are effectively nonlinear as a function of depth. In other words, the more submerged the tip is into the sample, the more spring-damper elements will be excited. This effectively increases the aggregate spring and damping

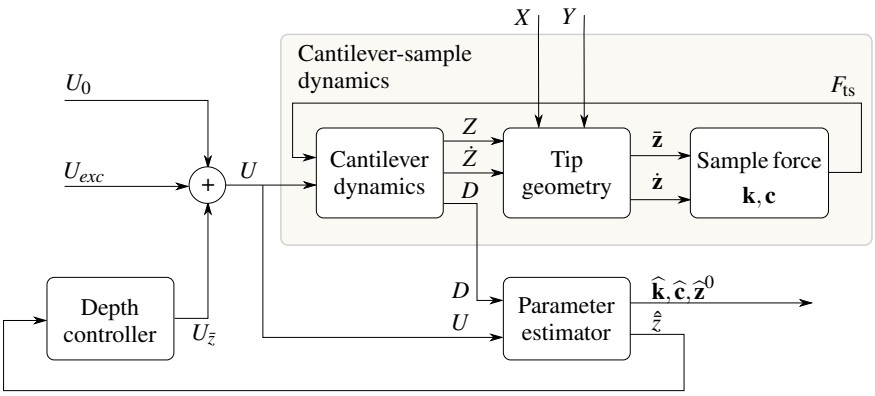

Fig. 3: Block diagram of the system dynamics, parameter estimator and depth controller. Only the cantilever deflection D and the vertical input position U are assumed measurable signals.

constants k and c, even though the element's true spring and damping constants k_i, c_i are the same. For an accurate representation of the sample properties the tip should thus be maintained at constant depth into the sample. For this reason a depth controller has been designed.

By employing the $\hat{z}^0$ estimate from the parameter identification, the indentation depth estimate is found from

$$\hat{\bar{z}} = Z - \hat{z}^0. \tag{25}$$

A simple I-controller is used to maintain desired depth $\bar{z}_{ref}$ described by

$$U_{\bar{z}} = k_i \int_0^t \left(\bar{z}_{ref} - \hat{\bar{z}}(\tau)\right) d\tau. \tag{26}$$

In summary, the input signal U is given by

$$U = U_0 + U_{exc} + U_{\bar{z}} \tag{27}$$

where U_0 is the constant initial position such that the tip starts submerged in the sample, U_{exc} is given by (24), and $U_{\bar{z}}$ by (26).

V. SIMULATION RESULTS

A simulation of the system as shown in Figure 3 has been implemented. Physical parameters have been chosen to approximate values of a real system. The cantilever was chosen with resonance frequency 20 kHz, effective mass 1.18×10^{-11} kg, damping coefficient 1.48×10^{-8} Ns/m, and spring constant 0.18 N/m. This equates to a cantilever quality (Q) factor of 100. The simulations were run using a variable-step solver with an average step size of 7.47 µs. This indicates a necessary sampling frequency for real-time implementation on the order of 130 kHz.

The sample was subdivided into a grid of 32×32 evenly spaced elements along the lateral axes representing the $1\,\mu\text{m} \times 1\,\mu\text{m}$ scanning area. Each element i is represented by its topography z_i^0, spring constant k_i, and damping constant c_i. The topography was designed to resemble a biological cell. The cantilever follows a raster pattern along the lateral axes, for a total of 20 scanlines. The scanning frequency along the x-axis is 0.2 Hz, with the entire scan thus taking 100 s. The reference depth $\bar{z}_{ref}$ was set to -50 nm. The excitation amplitudes a_1, a_2 were designed to oscillate the cantilever with amplitudes of 5 nm and 8 nm respectively.

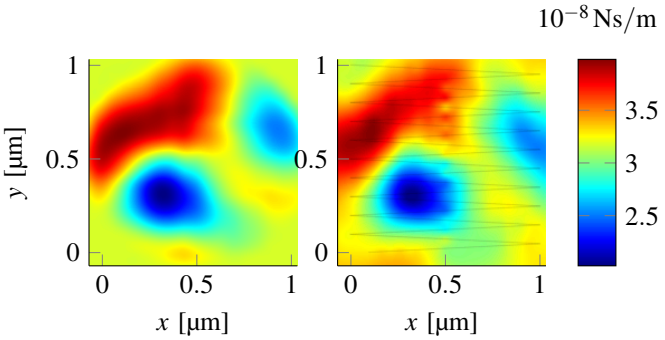

(a) Simulated, $\mathbf{c}$ **(b)** Estimated, $\hat{\mathbf{c}}$

Fig. 4: Damping constants (viscosity) mapped to the spatial domain. Demonstrates the effectiveness of the parameter estimator in identifying the simulated values. In **(b)** the scanning motion of the tip has been superimposed.

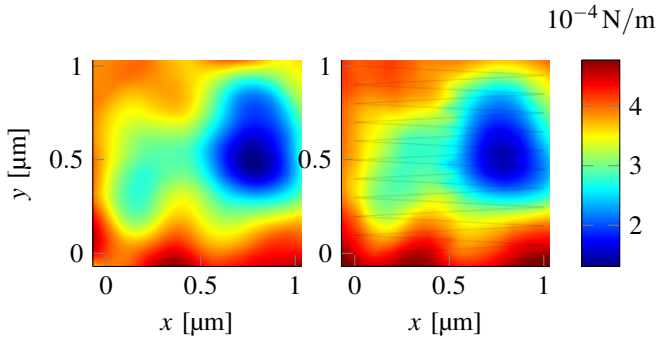

(a) Simulated, $\mathbf{k}$ **(b)** Estimated, $\hat{\mathbf{k}}$

Fig. 5: Spring constants (elasticity) mapped to the spatial domain.

The damping constant estimates can be seen in Figure 4, the spring constants in Figure 5, and the topography in Figure 6. The plots of the estimates have been produced by spline interpolation of the data between the scanning motion of the tip when mapping the data from the time domain

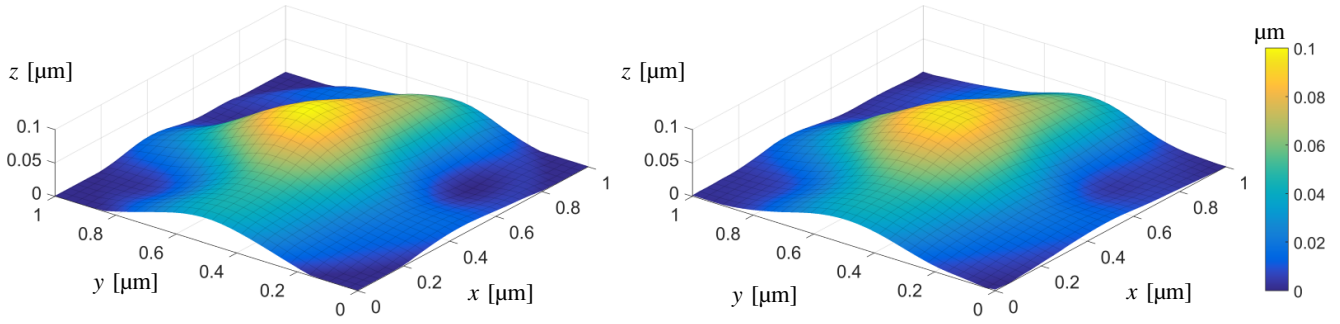

(a) Simulated, $\mathbf{z}^0$ **(b)** Estimated, $\hat{\mathbf{z}}^0$

Fig. 6: Topography of the sample.

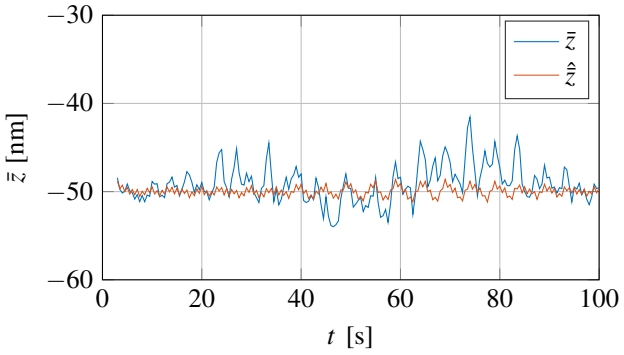

Fig. 7: Depth controller performance, showing the real indentation of the tip into the sample (blue), against the estimated indentation (red).

to the spatial domain. The images of the simulated values have been upscaled from their 32×32 data points for easier comparison. Since the estimates are aggregate values of the spring constants, the plots have been scaled by the average number of elements the tip is in contact with during the scan. This value can be determined from the tip geometry and the setpoint for the indentation depth.

The indentation depth is plotted against the estimated indentation depth in Figure 7. The estimated indentation is close to the setpoint at $-50\,\text{nm}$ which shows that the depth controller performs as intended. Some oscillation is expected and desired due to the excitation input signal U_{exc}. The actual indentation $\bar{z}$ has some larger peaks not caught by the estimator. This could be due to larger gradients in either the topography or spring constant that the estimator does not respond to sufficiently fast. This error should become smaller with slower scanning speeds. Additionally, significantly better performance is expected by increased tuning of the estimator.

VI. DISCUSSION

The depth controller is necessary for consistent results. Even for linear spring-damper systems such as presented here, the resulting aggregate of the spring and damping force acting on the tip becomes nonlinear in terms of indentation depth due to the tip geometry. Thus, a depth controller was designed to maintain constant indentation even in the presence of varying spring constants, and simulation results show the effectiveness of the controller. Traditional amplitude-modulated mode would not be sufficient as the amplitude will change as the elasticity of the sample changes. This controller scheme could also be useful in other applications where maintaining constant indentation in a heterogeneous material is desired.

A necessary sampling frequency around 130 kHz indicates that real-time operation of the procedure seems feasible. For experimental results only the parameter estimator and depth controller part of the simulation is needed, which considerably lowers the required computational effort. Additionally, the parts of the parameter estimator which are not necessary for use in the depth controller can be run offline after the experiments, which could make the procedure easier to implement in real-time.

For future work the system model can be extended to account for additional physical phenomena of the sample mechanics such as a cell membrane or nonlinear springs. The methodology easily allows for extensions as long as the unknown parameters appear linearly in the signal vector.

VII. CONCLUSIONS

Simulation results show the effectiveness of the method for determining elastic and viscous properties of a soft sample, as well as the topography. The method requires the AFM tip to be submerged into the sample during the scan, which makes it suitable for applications such as biological cells.

A modeling and identification approach is used for identifying the locally resolved spring and damping constants of the sample. The parameters are guaranteed to converge exponentially fast in dynamic mode AFM by employing the suggested input signal (27). Additionally, the identification method simultaneously provides a true topography estimate overcoming the challenge of the tip being submerged and the spring parameters varying during the entire scan.

Since the methodology continuously scans across the surface in a raster pattern rather than tapping in and out of the sample at discrete number of points, the total scan speed is significantly reduced compared to earlier results and the spatially resolved parameter resolution is increased.

REFERENCES

[1] S. Suresh, "Biomechanics and biophysics of cancer cells," *Acta Materialia*, vol. 55, no. 12, pp. 3989–4014, 2007.

[2] C. T. Lim, E. H. Zhou, and S. T. Quek, "Mechanical models for living cells - A review," *Journal of Biomechanics*, vol. 39, no. 2, pp. 195–216, 2006.

[3] B. D. Hoffman and J. C. Crocker, "Cell mechanics: dissecting the physical responses of cells to force." *Annual review of biomedical engineering*, vol. 11, pp. 259–288, 2009.

[4] K. Haase, A. E. Pelling, and K. Haase, "Investigating cell mechanics with atomic force microscopy," *Journal of The Royal Society Interface*, vol. 12, 2015.

[5] I. Sokolov, M. E. Dokukin, and N. V. Guz, "Method for quantitative measurements of the elastic modulus of biological cells in AFM indentation experiments," *Methods*, vol. 60, no. 2, pp. 202–213, 2013.

[6] D. J. Müller and Y. F. Dufrêne, "Atomic force microscopy: a nanoscopic window on the cell surface." *Trends in cell biology*, vol. 21, no. 8, pp. 461–469, 2011.

[7] N. Guz, M. Dokukin, V. Kalaparthi, and I. Sokolov, "If Cell Mechanics Can Be Described by Elastic Modulus: Study of Different Models and Probes Used in Indentation Experiments," *Biophysical Journal*, vol. 107, no. 3, pp. 564–575, 2014.

[8] R. Garcia and R. Perez, "Dynamic atomic force microscopy methods," *Surface science reports*, vol. 47, no. 6-8, pp. 197–301, 2002.

[9] M. R. P. Ragazzon, J. T. Gravdahl, and A. J. Fleming, "On Amplitude Estimation for High-Speed Atomic Force Microscopy," in *American Control Conference*, Boston, USA, 2016.

[10] M. G. Ruppert, K. S. Karvinen, S. L. Wiggins, and S. O. R. Moheimani, "A Kalman Filter for Amplitude Estimation in High-Speed Dynamic Mode Atomic Force Microscopy," *Control Systems Technology, IEEE Transactions on*, vol. 24, no. 1, pp. 276–284, 2016.

[11] T. G. Kuznetsova, M. N. Starodubtseva, N. I. Yegorenkov, S. A. Chizhik, and R. I. Zhdanov, "Atomic force microscopy probing of cell elasticity," *Micron*, vol. 38, pp. 824–833, 2007.

[12] C. T. McKee, J. A. Last, P. Russell, and C. J. Murphy, "Indentation versus tensile measurements of Young's modulus for soft biological tissues." *Tissue engineering. Part B, Reviews*, vol. 17, no. 3, pp. 155–164, 2011.

[13] A. Raman, S. Trigueros, A. Cartagena, A. P. Z. Stevenson, M. Susilo, E. Nauman, and S. A. Contera, "Mapping nanomechanical properties of live cells using multi-harmonic atomic force microscopy." *Nature nanotechnology*, vol. 6, no. 12, pp. 809–14, 2011.

[14] A. X. Cartagena-Rivera, W.-H. Wang, R. L. Geahlen, and A. Raman, "Fast, multi-frequency, and quantitative nanomechanical mapping of live cells using the atomic force microscope," *Scientific Reports*, vol. 5, p. 11692, 2015.

[15] M. Radmacher, R. W. Tillmann, and H. E. Gaub, "Imaging viscoelasticity by force modulation with the atomic force microscope." *Biophysical journal*, vol. 64, no. 3, pp. 735–742, 1993.

[16] M. Lekka, K. Pogoda, J. Gostek, O. Klymenko, S. Prauzner-Bechcicki, J. Wiltowska-Zuber, J. Jaczewska, J. Lekki, and Z. Stachura, "Cancer cell recognition - Mechanical phenotype," *Micron*, vol. 43, no. 12, pp. 1259–1266, 2012.

[17] M. R. P. Ragazzon, M. Vagia, and J. T. Gravdahl, "Cell Mechanics Modeling and Identification by Atomic Force Microscopy," in *7th IFAC Symposium on Mechatronic Systems*, Loughborough, UK, 2016.

[18] D. R. Sahoo, A. Sebastian, and M. V. Salapaka, "An ultra-fast scheme for sample-detection in dynamic-mode atomic force microscopy," in *2004 NSTI Nanotechnology Conference and Trade Show - NSTI Nanotech*, vol. 3, 2004, pp. 11–14.

[19] P. A. Ioannou and J. Sun, *Robust adaptive control*. Upper Saddle River, NJ: Prentice Hall, 1996.

[20] M. Krstic, I. Kanellakopoulos, and P. Kokotovic, *Nonlinear and adaptive control design*. New York, NY: John Wiley & Sons, Inc., 1995.